THE JOURNAL OF PHYSICAL CHEMISTRY B

Article

pubs.acs.org/JPCB

First-Principles Study on Core-Level Spectroscopy of Arginine in Gas and Solid Phases

Hongbao Li,[†,‡] Weijie Hua,[‡] Zijing Lin,*[,†] and Yi Luo*[,†,‡]

[†]Hefei National Laboratory for Physical Sciences at Microscale and Department of Physics, University of Science and Technology of China, Hefei, Anhui, 230026, China

[‡]Department of Theoretical Chemistry and Biology, School of Biotechnology, Royal Institute of Technology, S-106 91 Stockholm, Sweden

ABSTRACT: First-principles simulations have been performed for near-edge X-ray absorption fine-structure (NEXAFS) spectra of neutral arginine at different K-edges in the solid phase as well as X-ray photoelectron spectra (XPS) of neutral, deprotonated, and protonated arginines in the gas phase. Influences of the intra- and intermolecular hydrogen bonds (HBs) and different charge states have been carefully examined to obtain useful structure−property relationships. Our calculations show a noticeable difference in the NEXAFS/XPS spectra of the canonical and zwitterionic species that can be used for unambiguously identifying the dominant form in the gas phase. It is found that the deprotonation/protonation always results in red/blue shifts of several electronvolts for the core binding energies (BEs) at all edges. The normal hydrogen bond Y−H···X (X, Y = N, O) can cause a blue/red shift of ca. 1 eV to the core BEs of the proton acceptor X/donor Y, while the weak C−H···Y hydrogen bond may also lead to a weak red shift (less than 1 eV) of the C1s BEs. Moreover, the influence of intermolecular interactions in the solid state is reflected as a broadening in the σ^* region of the NEXAFS spectra at each edge, while in the π^* region, these interactions lead to a strengthening or weakening of individual transitions from different carbons, although no evident visual change is found in the resolved total spectra. Our results provide a better understanding of the influences of the intra- and intermolecular forces on the electronic structure of arginine.

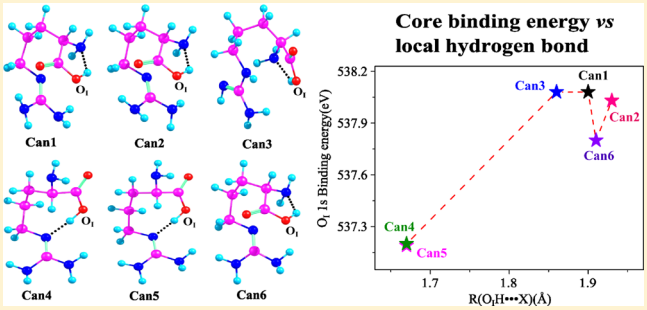

1. INTRODUCTION

Various core-level spectroscopies provide efficient tools in probing the electronic structure of biomolecules. These techniques are element-selective, sensitive to the local chemical environment, and can differentiate the oxidation states, charge states, chemical bonding, and hydrogen bonding, etc.[1] Particularly for amino acids, their X-ray photoelectron spectra (XPS) and near-edge X-ray absorption fine structure (NEXAFS) spectra have been extensively measured in the gas phase,[2−12] aqueous solution,[13−17] and solid state.[5,18−24] Among all the measurements, the gas-phase study might be the most difficult because the experiments are usually performed at high temperature and low vapor pressure at which conditions the samples are very easy to decompose. Although gas-phase soft-X-ray experiments have covered many amino acids or their analogs (for example, glycine, proline, methionine,[7−9] alanine, threonine,[10] glycyl-glycine,[11] phenylalanine, tyrosine, and tryptophan[12]), such studies are far from exhaustive; for instance, no data are available for arginine due to the extreme difficulty in thermal evaporation of the sample. The importance of a gas-phase investigation over a condensed-phase study is the ability to filter out all environmental factors and to capture the inherent properties of amino acids. It is well-known that the intermolecular interactions from the solvent (liquid phase) or neighboring amino acid molecules (solid phase) can have a significant impact on the chemical and electronic structures. With the results of the isolated amino acids as reference, one can understand better the intramolecular forces that stabilize their structure or the more complex peptides and proteins constructed from them. In this context, theoretical studies are particularly useful in revealing the underlying structure−property relationships.

The challenge of theoretical study for an amino acid in a vacuum lies in the coexistence of many isomers which have close energies and comparable populations. Early theoretical study was limited to one fixed, optimized geometry,[9] while a better description needs to include more low-lying structures especially considering the high-temperature experimental conditions. An efficient way is thus demanded to sample out a limited number of lowest-lying configurations from the full configuration space, and the final spectrum is computed according to the equilibrium distribution of those few isomers, i.e., as an average weighted by the Boltzmann factor. The sampling is usually done by varying the internal rotational

Received: March 14, 2012
Revised: September 25, 2012
Published: September 27, 2012

degrees of freedom. It is more difficult for arginine since the guanidine group introduces more rotational degrees of freedom than other amino acids. Moreover, it also brings in variations in the charge states, which had set a longtime debate on whether the canonical or the zwitterionic form dominantly exists in the gas phase.[25−27] These two neutral forms, together with the protonated and deprotonated arginines, are illustrated in Scheme 1. For this molecule, efforts on the isomer searching

Scheme 1. Schematic Illustration of the Arginine in (a) Canonical, (b) Zwitterionic, (c) Protonated, and (d) Deprotonated Forms with Heavy Atoms Labeled

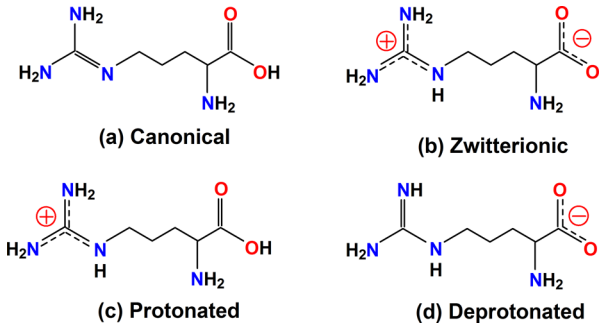

have been made in the past few decades. Rak et al.[26] used a simple genetic algorithm (SGA)[28] to vary selected geometrical parameters, and the trial structures were optimized by a semiempirical PM3 and ab initio method. Schlund et al.[29] applied a strategy to identify the most stable conformers of arginine by means of a force-field-based conformational search strategy in combination with high-level geometry optimizations. On the basis of some conformers found by Rak et al., Ling et al.[27] found lots of new low-energy structures of canonical, zwitterionic, and protonated arginine using a "step-by-step" strategy. This provides the most accurate structures available up till now.

Herein, taking advantage of the early success of the isomer searching, we choose only a few lowest-lying isomers of neutral arginine obtained from the early study,[27] as well as employ the same strategy for deprotonated arginine, and then calculate the NEXAFS and XPS spectra at all relevant absorption edges (C, N, and O) by the density functional theory (DFT). Special attention is paid to the effects of the hydrogen bonding (HB) since it is the major nonbonding interaction in this system. In amino acids, the hydrogen bonds contain the normal Y−H···X (X, Y = N, O) type HB and the weaker C−H···X hydrogen bond, which are, respectively, termed as red- and blue-shifting HBs in the vibrational spectroscopy.[30] Besides, there is also a weaker dihydrogen bond C−H···H−X.[31] It would be interesting to see their influences in the X-ray region. Since the difference in charge states can be qualitatively determined by the XPS spectrum,[32] such studies may help resolve the debate on dominant forms when new experiments are available.

Another theme of this work is to examine the solid-state effect of arginine. In the solid state, arginine exists in the zwitterionic form, and the structure is mainly stabilized by the electrostatic interaction and intermolecular hydrogen bonding between the zwitterions. Comparison with the gas-phase spectra can reflect the effects of these interactions. Since all early experimental NEXAFS spectra on arginine were measured in the solid state,[22−24] corresponding calculations should be helpful to verify and to understand the spectral features. In practice, it can be done by constructing a reasonably large model to include the necessary local environment, which is usually done by using either a truncated cluster[33−37] or a periodic supercell.[38−41]

This article is organized as follows. In Section 2, we describe the computational methods for NEXAFS spectroscopy of arginine in the solid state as well as the NEXAFS and XPS spectra in the gas phase. Section 3 presents the spectral results and discussions on the structure−property relationships. Concluding remarks are finally given in Section 4.

2. COMPUTATIONAL METHODS

2.1. Solid-State NEXAFS. NEXAFS spectra are calculated based on the crystal structure of arginine monohydrate, which has *Pbca* space group symmetry and contains only one nonequivalent arginine residue in each cell.[42] A truncated cluster model is constructed using the technique which has been given elsewhere.[43] Briefly, we choose one arginine as the central residue and cap it with neighboring residues (arginine or crystal water) within a distance threshold ξ = 3.0 Å to obtain the model. (Here the residue−residue distance is defined as the minimum atom i − atom j distance with i and j atoms in the central and surrounding residues, respectively.) Such a threshold is enough to include all residues which form hydrogen bonds with the central one.[43]

Spectra at the C1s, N1s, and O1s edges are then calculated by using the equivalent core hole (ECH, or Z + 1) approximation.[44−47] Within this approximation, the core-excited atom is replaced with the next element in the periodic table, while the number of electrons is kept the same as in the ground state. For example, the excited oxygen atom O* is replaced by F^+. This method is usually considered as a further approximation to the full core hole (FCH) method. The underlying physics is that the increased nuclear charge by one (Z + 1) creates an electric potential similar to a core hole, as seen from the outer-shell electrons.[47] It has been demonstrated successfully in the prediction of K-edge spectra of various systems including organic or biological molecules[42,48,49] and nanomaterials.[50−52] This has been implemented by using a combination of GAUSSIAN 09 package[53] and BioNano-Lego code.[54] The former generates the molecular orbital (MO) coefficients and atomic orbital dipole integrals from a single-point calculation, and the latter calculates the oscillator strength for transition $i \rightarrow n$ by using the following working formula

$$f_{ni} = \frac{2m\varepsilon_{ni}}{3\hbar^2} \sum_{\hat{O}=x,y,z} |\langle \psi_n|\hat{O}|\psi_i\rangle|^2 \quad (1)$$

Here $\psi_{i,n}$ denotes a pair of molecular orbitals of the ECH-state wave function; $\varepsilon_{ni} = \varepsilon_n - \varepsilon_i$ represents the orbital energy difference; and the average over x, y, and z is to account for the random orientation of molecules in a powder polycrystal sample. Calculations are performed at the unrestricted DFT level,[55] and the B3LYP[56] and M062X[57] functionals are both employed for comparison. The triple-ζ quality individual gauge for localized orbital (IGLO-III) basis set[58] is chosen for the excited atom (five basis functions for the d-shell), the 6-31+G basis set for the heavy atoms in all charge centers (i.e., the guanidine and carboxyl groups), and the 6-31G basis set for the rest. With the stick spectra provided, they are broadened by a Gaussian line shape with full-width-at-half-maximum (fwhm) of 0.7 eV for the first few electronvolts above the absorption edge, linear-increasing fwhm up till 8.0 eV (12.0 eV for the O edge)

dx.doi.org/10.1021/jp302309u | J. Phys. Chem. B 2012, 116, 12641−12650

Table 1. Percent Shares of the Neutral or Deprotonated Arginine Conformers in Their Respective Equilibrium Mixtures at Various Temperatures

molecule	isomer	T = 98 K	T = 198 K	T = 298 K	T = 443 K
neutral arg.[a]	Can1	14.7	10.6	7.6	5.3
	Can2	5.0	11.8	12.7	11.6
	Can3	0.6	2.6	3.4	3.3
	Can4	39.8	31.4	25.6	19.8
	Can5	38.8	33.3	28.1	22.4
	Can6	0.9	5.3	8.1	9.3
	Z1	0.0	0.0	0.0	0.0
deprotonated arg.	Dp1	98.1	71.3	44.6	27.2
	Dp8	0.9	7.8	11.4	12.1
	Dp18	0.1	7.1	18.5	28.3

[a]The energy data were taken from ref 27 to calculate the percent shares. Can1−Can6 were denoted as c1−c6 and Z1 as z21 in the reference.

in the next 2.0 eV, and fwhm = 8.0 eV (12.0 eV for the O edge) for the region beyond. Each convoluted spectrum has been directly calibrated to the corresponding experimental spectrum of arginine powders[24] by aligning the first π^* peak. It is noticed that our concern in this work is mainly on the π^* region, and a large broadening simply employed in the σ^* region is quite empirical. For a more adequate description of the electronic transitions to the continuum, one is recommended to other approaches which make use of periodic supercells and numerical convergence in the electron momentum space (see, for example, refs 59−62).

2.2. Gas-Phase XPS and NEXAFS. To examine the gas-phase XPS and NEXAFS spectra, we have taken representative lowest-energy isomers from the early studies.[27] Particularly, seven neutral (six in canonical and one in zwitterionic forms) and one protonated arginine are selected.[63] Additionally, three depronoated arginine structures are generated following the same step-by-step method[27] with the GAUSSIAN 09 package.[53] For these small molecules, the C1s, N1s, and O1s NEXAFS and XPS spectra are calculated by using the StoBe program[64] at the DFT level with the gradient-corrected Becke (BE88) exchange[65] and Perdew (PD86) correlation functionals.[66] The IGLO-III basis set[58] is set for the excited atom; the triple-ζ plus valence polarization (TZVP) basis set is employed for the others; and miscellaneous auxiliary basis sets are also set for all atoms. To facilitate the convergence of the core-hole state, for those nonexcited atoms that are of the same element as the excited one, their 1s electrons are modeled by model core potentials. The ionization potentionals (IPs) are computed via a ΔKohn−Sham (ΔKS) approach,[67,68] i.e., the energy difference of the FCH and ground state (GS)

$$\mathrm{IP} = {}^{N-1}E_{\mathrm{FCH}} - {}^{N}E_{\mathrm{GS}} \quad (2)$$

The XPS spectra are simply obtained by a Gaussian convolution of the ionization potentionals (IPs) with a fwhm of 0.1 eV. The NEXAFS spectra are calculated with the FCH approximation in combination with a double basis set technique in which an augmented diffuse basis set (19s, 19p, 19d) is added for the excited atom to obtain a proper representation of the Rydberg and continuum excited states.[69] All calculated spectra are calibrated by aligning the 1s → LUMO (lowest unoccupied MO) transition to that obtained from the ΔKS approach, i.e.

$$\varepsilon^{\Delta\mathrm{KS}}_{\mathrm{LUMO,1s}} = {}^{N}E_{\mathrm{1s}\rightarrow\mathrm{LUMO}} - {}^{N}E_{\mathrm{GS}} \quad (3)$$

Relativistic effects of +0.2, +0.3, and +0.4 eV for the C, N, and O edges, respectively, are used to produce the overall shift of the spectra.[69] It is noticed that the C1s → $\pi^*_{\mathrm{C=O}}$, N1s → π^*_{NC}, and O1s → $\pi^*_{\mathrm{C=O}}$ transitions of neutral arginine are normally found at 288.4, 402.3, and 532.2 eV, respectively, in many gas-phase NEXAFS experiments.[2,15,16] To be more relevant to the future experiments, we have further shifted our calculated spectra to align with the first experimental π^* peaks, which correspond to +1.18, +0.13, and +0.73 eV for C, N, and O edges, respectively. Such a shift does not have particular physical meaning but is purely a practical solution to match experiment. Stick NEXAFS spectra are convoluted with the Gaussian function with fwhm of 0.1 and 1 eV below and above the IPs. The spectra of the neutral or deprotonated arginine are obtained as a summation weighted by their relative abundance. The experimental temperature (443 K) is used for both spectra, and additionally, three more temperatures, 98, 198, and 298 K, are employed for the XPS spectra to see the temperature effect. The percent shares of isomers at each temperature have been given in Table 1.

3. RESULTS AND DISCUSSION

3.1. NEXAFS of Arginine Monohydrate Crystal. Figure 1a displays the constructed cluster model for the arginine monohydrate crystal, which contains 382 atoms including 14 zwitterionic arginines and 6 crystal waters. The central arginine acts as a proton acceptor at the N/O terminal and donor at the guanidine site. Calculated NEXAFS spectra by the B3LYP and M062X functionals are shown in Figures 1b and 1c, respectively, compared with experimental results from solvent-free polycrystalline powder films.[24] Generally, theoretical spectra by both functionals match well with the experiment, with all main features reproduced. In panel a, our results clearly show (denoted by arrows) that the experimental pre-edge at 285.3 eV comes from the carboxylic carbon (C_1) π^* resonances, while the shoulder structure at 287.6 eV corresponds to excitations from multicarbon centers. The experimental double-peak split by about 0.6 eV (at 288.6 and 289.2 eV) is roughly reproduced. Evidently, the α carbon (C_2) exhibits a sharp peak in this region, while all other carbons also have considerable contributions here. Such a complexity sets a high accuracy requirement of each individual atom-specific spectrum (in both the spectral shapes and the relative positions) to reproduce the total fine structure by theory. However, for such an ionic crystal with multilocalized charge centers, the spatial fluctuation of electron density makes it difficult to be described by DFT functionals. Although early

dx.doi.org/10.1021/jp302309u | J. Phys. Chem. B 2012, 116, 12641−12650

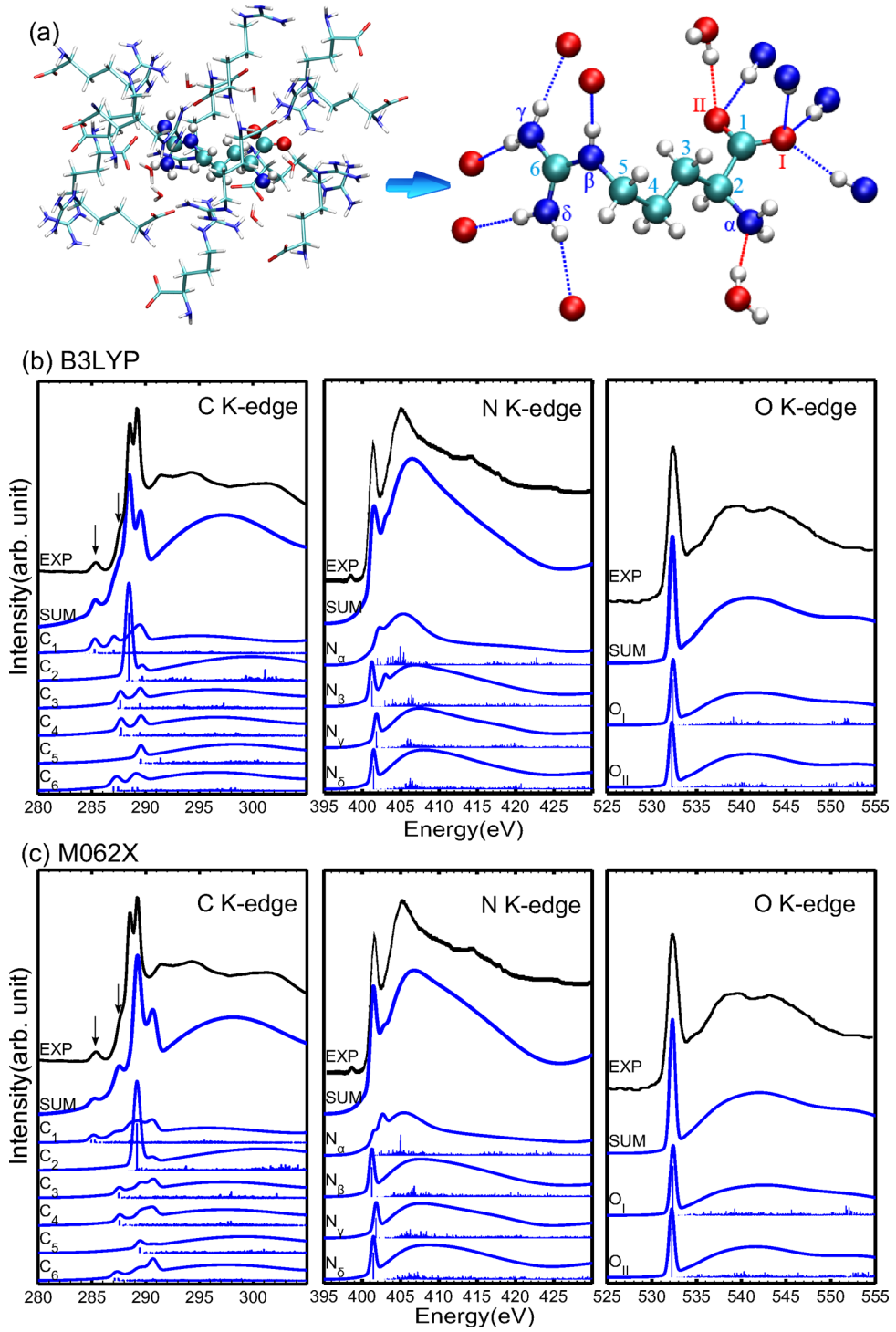

Figure 1. (a) Cluster model of arginine monohydrate crystal used for spectral calculation and close-up of the local hydrogen bonding for the central arginine. Total and atom-specific NEXAFS spectra at the C, N, and O K-edges calculated with (b) B3LYP and (c) M062X functionals compared with experiment.[24]

works showed that the functional dependence of soft X-ray spectra is small for molecules[70] and molecular crystals,[71,43] one can see that for this system the results are slightly more sensitive to different functionals, with B3LYP predicting relatively better peak positions than M062X. The N1s spectrum is featured by a strong, single π^* resonance at ca. 401.4 eV and a strong σ^* peak beyond. The strong transitions are due to the structural similarity of the four nitrogens. This agrees well with our early experience in DNA that a primary (here, N_α, N_γ, N_δ) or secondary (here, N_β) amine nitrogen does not show different absorption energies.[49] Additionally, the hydrogen bond network also makes them even less distinguishable.[43] The O1s spectrum is featured by a narrow, single π^* resonance at ca. 532.4 eV and a wide σ^* peak beyond. The above discussions show that the cluster model based on the crystal structure of arginine monohydrate are capable of predicting the NEXAFS spectra of a powder sample.

dx.doi.org/10.1021/jp302309u | J. Phys. Chem. B 2012, 116, 12641−12650

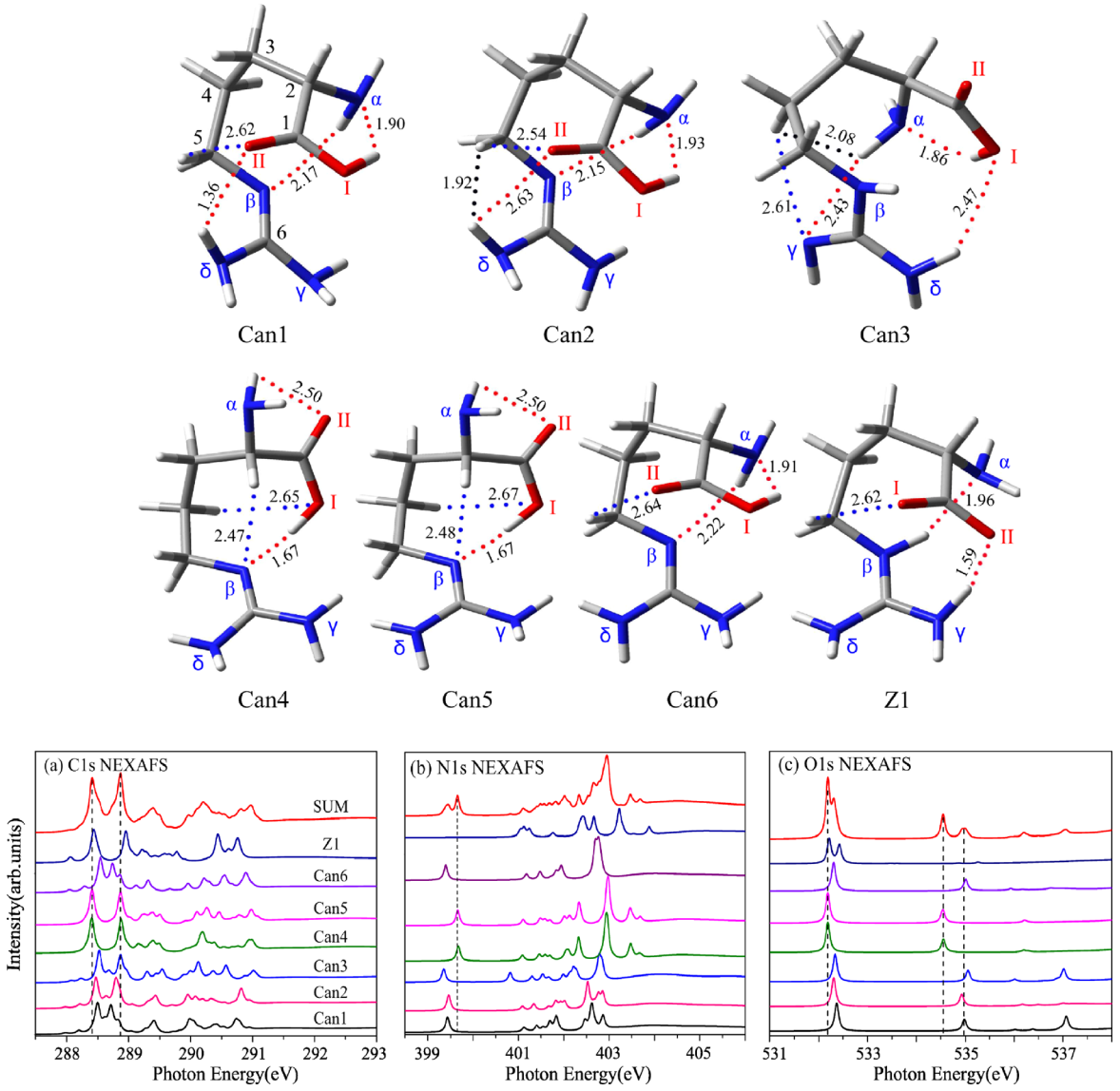

Figure 2. Calculated (a) C1s, (b) N1s, and (c) O1s NEXAFS spectra of lowest-energy conformers of neutral arginine (Can1−Can6 and Z1, respectively, denote the canonical and zwitterionic forms) as well as the averaged spectra at 443 K according to their equilibrium distributions. Structures are depicted on top of the spectra, and different types of intramolecular hydrogen bonds (distances in Å) are indicated by dotted lines: red, Y−H···X (X, Y = N, O); blue, C−H···X (X = N, O); black, C−H···H−X (X = N, O).

3.2. Gas-Phase NEXAFS Spectra. Figure 2 presents the individual NEXAFS spectra of the six canonical (denoted as Can1−Can6) and one zwitterionic (Z1) arginine isomers, together with the averaged spectrum of neutral arginine at 443 K. Since Z1 makes almost no contributions to the average spectra (see Table 1) due to its high energy, the average spectra can be just considered as those of the canonical form. A visible spectral difference can be found between the two forms at all edges. In the C1s edge, both show a double π^* peak at ca. 288−289 eV, which comes from the transitions C_1 1s→$\pi^*_{C=O}$ and C_6 1s→$\pi^*_{C=N}$, respectively. Z1 exhibits a slightly wider splitting of 0.6 eV (288.4 and 289.0 eV) than the 0.4 eV (288.4 and 288.8 eV) of the canonical form. More significant differences are found in the N spectra. The canonical form shows a π resonance at 399.4−399.7 eV, while in Z1 this is blue-shifted to 401.1−401.2 eV. In the O spectra, both forms show a π resonance at 532.2 eV. While only the canonical isomer exhibits a resonance at 534.6−535.0 eV, which mainly comes from transitions O_I 1s→$\pi^*_{C=O}$ and O_I, O_{II} 1s→3s/σ^*_{OH}. Such a spectral difference can be useful to distinguish the dominant forms in the gas phase.

Meanwhile, one can get the influence of the solid-state effect by comparing the spectra of Z1 with the solid-state spectra. In the C spectra, although both exhibit a double π^* peak of 1.0 eV separation and at nearly the same region, they come from different sources (C_1 and C_2 in the solid state; C_1 and C_6 in the gas phase). This illustrates that the intermolecular HB network in the solid state (especially that around C_2 and C_6) as well as the electrostatic interactions strongly influence the electronic structure of the central residue. The N or O spectra seem to be less influenced: they show π^* transitions roughly at the same regions. Anyway, the solid state always shows much broader σ^* transitions in all edges, which is simply due to a denser density of states and more possibility for transitions to states which span multiple molecules at high energy.

dx.doi.org/10.1021/jp302309u | J. Phys. Chem. B 2012, 116, 12641−12650

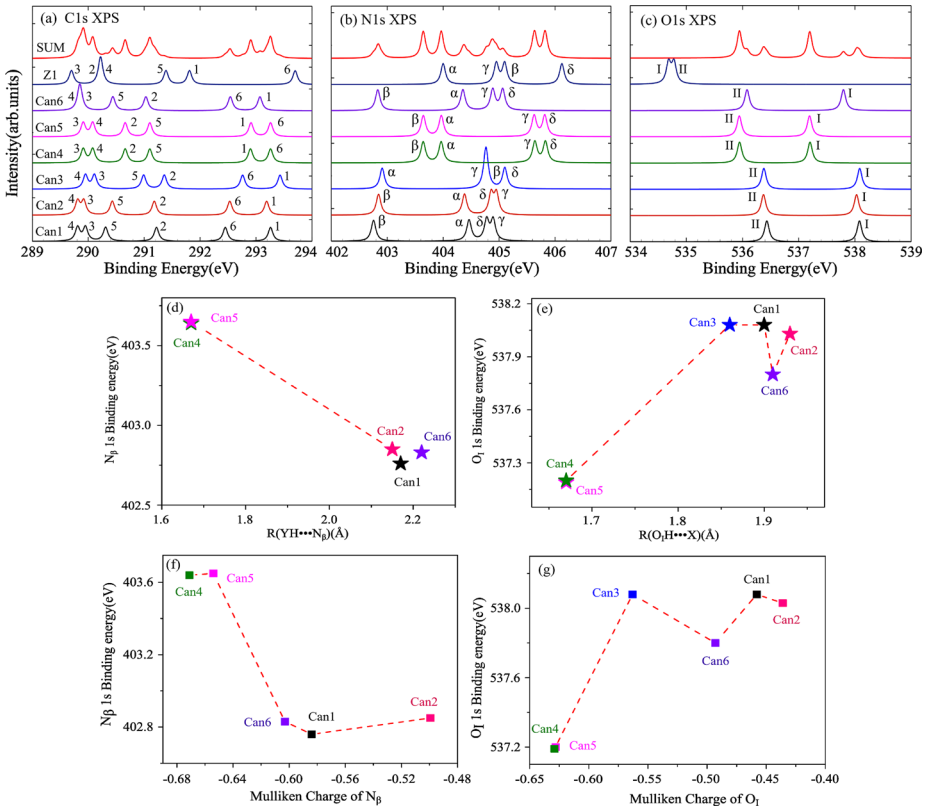

Figure 3. Calculated (a) C1s, (b) N1s, and (c) O1s XPS spectra of lowest-energy conformers of neutral arginine isomers as well as the averaged spectra at 443 K according to their equilibrium distributions. Plot of core binding energies of (d) N_β and (e) O_I versus the local HB lengths [R(Y−H···N_β) and R(O−H···X), respectively] in different isomers. Here Y = N_α, X = N_α for Can1, Can2, and Can6, and Y = O_I, X = N_β for Can4 and Can5; see structures in Figure 2 and text for more details. Plot of core binding energies of (f) N_β and (g) O_I versus the (ground-state) Mulliken charge population on the excited atom.

3.3. Gas-Phase XPS. *3.3.1. Neutral Arginine.* C1s, N1s, and O1s XPS spectra of each neutral isomer are plotted in Figures 3a−3c, together with the averaged spectra at 433 K. The zwitterionic isomer Z1 exhibits visible chemical shifts of K-shell binding energies (BEs) to the six canonical isomers. At all edges, we find that the lowest peak of Z1 always starts from a different energy region than the canonical isomers. In the C edge, the lowest peak is slightly red-shifted by 0.1−0.3 eV. Much larger shifts are found for nitrogens and oxygens: such peaks being blue-shifted by 0.4−1.2 eV and red-shifted by 1.3−1.8 eV, respectively. Results show that the core BE shifts are sensitive to different charge states, and an increase of electron population on the excited atom leads to a smaller BE. Qualitatively, this is because the increase of electron population (e.g., from COOH to COO^- for oxygens) enhances the screening of the K-shell electrons by the outer electrons.[72] Therefore, the core BE shifts provide a promising way to distinguish the canonical or the zwitterionic isomers. If corresponding experiments become available in the future, the XPS spectra, especially at the O edge, are expected to unambiguously resolve the debate on the dominant form in the gas phase.[25−27] An interesting relation has also been found between the core BE shifts and local hydrogen bonds (formed with the participant of the excited atom). For simplicity, analysis here is limited only for the canonical isomers. We find that a hydrogen bond C−H···X (X = N, O) usually leads to a red shift of C1s BEs. As an example for carbon C_2, a hydrogen bond C_2−H···N_β is formed in isomers Can4 and Can5, and the BEs are about 0.4−0.7 eV lower than the other canonical isomers. Another example is carbon C_5: the formation of a hydrogen bond C_5−H···O_{II} in Can1, Can2, and Can6 leads to a red-shift of BE for C_5 (with respect to the other canonical isomers). Note that a special dihydrogen bond C_5−H···H−N_δ is also formed in conformer Can2, but its influence is found to be weak.

Meanwhile, at the nitrogen and oxygen sites, multiple HBs (up to two) are found, and our analysis is limited for cases where one strong HB dominates. It is found that the conventional hydrogen bond Y−H···X (X, Y = N, O) roughly causes a blue (red) shift of core BE of the proton acceptor X (proton donor Y). For instance, we illustrate the core BEs of N_β and O_I versus the HB length (for cases with two HBs, the stronger one is chosen) in Figures 3d and 3e, respectively. In either panel, although no monotonic relation is found due to complex geometrical factors, isomers Can4 and Can5 distinguish well from the others due to a strong hydrogen bond O_I−H···N_β formed. As a result, the core BEs of N_β in these two isomers (403.6 eV) are about 0.8 eV higher than the other isomers (402.8 eV), and that of O_I (537.2 eV) is 0.6−0.9 eV lower than the other isomers (537.8−538.1 eV). This shows that core BE shifts can qualitatively reflect the local HBs. Note that Can3 is not present in Figure 3d due to its special geometry of the guanidine group compared with other canonical isomers (see structures in Figure 2); the extra hydrogen at N_β leads to a much larger binding energy of 404.8 eV, which is comparable with the 405.1 eV in Z1. Alternatively, we also examine the relationship between the core BE and the Mulliken charge population on the excited atoms and present

dx.doi.org/10.1021/jp302309u | J. Phys. Chem. B 2012, 116, 12641−12650

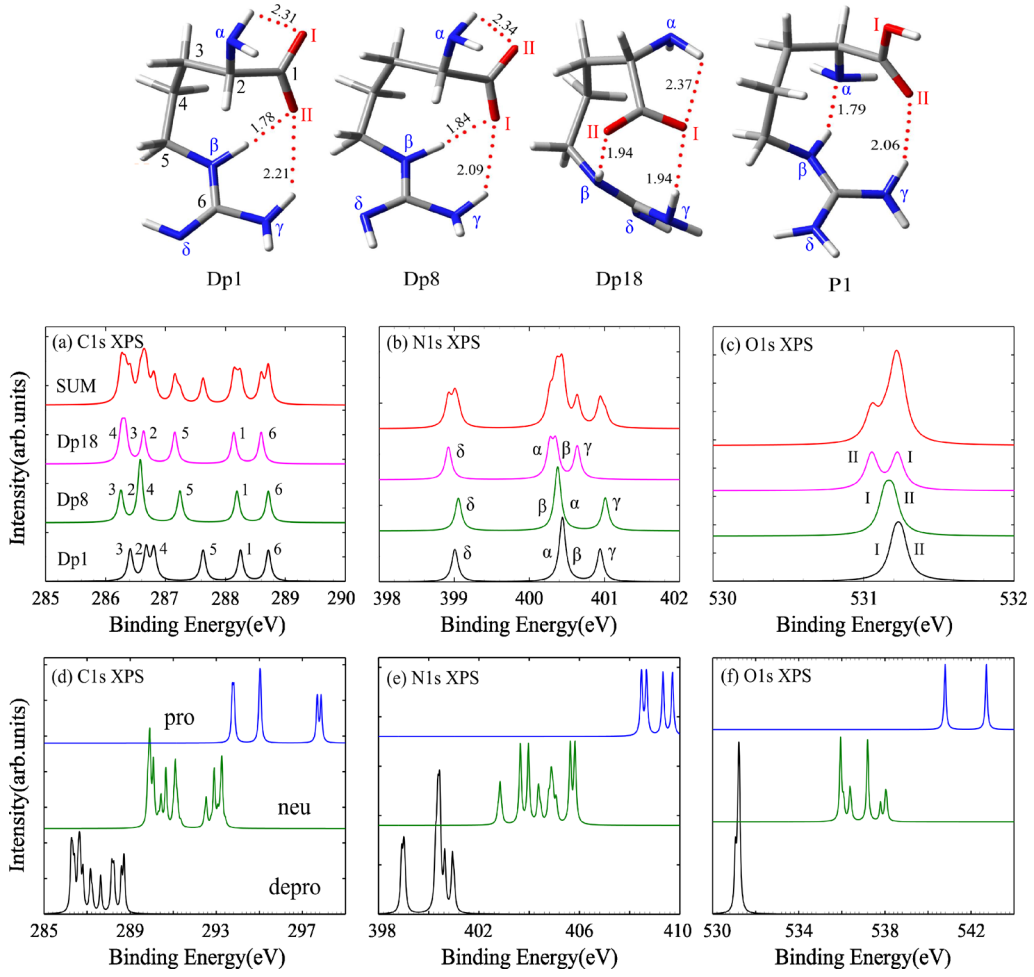

Figure 4. Calculated (a) C1s, (b) N1s, and (c) O1s XPS spectra of lowest-energy conformers of depronoated (Dp1, Dp8, Dp18) and protonated (P1) arginine isomers as well as the averaged spectra at 443 K according to their equilibrium distributions. Comparison of averaged spectra at 443 K for prononated, neutral, and deprononated arginines at the (d) C1s, (e) N1s, and (f) O1s edges. Structures are depicted on top of the spectra. All intramolecular hydrogen bonds are of Y−H···X type (X, Y = N, O) and are indicated by red dotted lines (distances in Å).

the results for N_β and O_I in Figures 3e and 3f, respectively. One can find that Can4 and Can5 which possess large binding energies also have more negative charges on the excited atoms. However, such an analysis in general is also quite qualitative since no monotonic relationship is found here. The reason is simply the complex geometric difference of the isomers, as stated above.

3.3.2. Deprotonated and Protonated Arginines. XPS spectra of the three deprotonated arginine isomers (denoted as Dp1, Dp8, and Dp18) as well as the averaged spectra at 443 K are depicted in Figures 4a−4c. For each isomer, the disappeared proton enlarges the discrepancy of the local chemical environment of N_γ and N_δ and causes a much larger separation (ca. 1.7−1.9 eV) of the core binding energies as compared with the neutral ones (ca. 0.2 eV). By contrast, the local environment of the two oxygens gets closer, and they almost exhibit identical binding energy at ca. 531.2 eV. The averaged spectra are compared with the neutral and protonated arginines in Figures 4d−4f. One can see that the charge states strongly influence the core binding energies, and at all edges deprotonation and protonation always lead to a red and blue shift of the core binding energies. For instance, at the O1s edge, the protonated isomer P1 has a binding energy of 540.8−542.7 eV. Neutral isomers cover about 535.9−538.0 eV, while the deprotonated isomers reach about 531.2 eV. Our result is consistent with early combined experimental and theoretical XPS study for aqueous glycine.[17] This is because a more negative charge population increases the screening of the K-shell electrons by the outer electrons (i.e., the nuclear potential is decreased[17]) and leads to a smaller core binding energy.[72]

3.3.3. Temperature Effect. Figure 5 compares the averaged spectra for neutral and deprontonated arginines at four different temperatures. Evidently, a lower temperature strengthens the contribution of Can4 and Can5 which have the lowest free energies (ca. 0.4−0.7 kcal/mol lower than the others). Each isomer contributes only around 20% at 443 K, while the ratio reaches almost 40% at 98 K. Generally, the peak positions do not show an evident difference when lowering the temperature. Changes happen with the peak intensities: the spectra become even sharper at lower temperatures due to more pure populations. Meanwhile, some weak structures also disappear. For example, in the O spectra of deprotonated arginine (panel c2), the shoulder structure at 531.1 eV (mainly contributed from Dp18) gradually disappears when lowering the temperature.

dx.doi.org/10.1021/jp302309u | J. Phys. Chem. B 2012, 116, 12641−12650

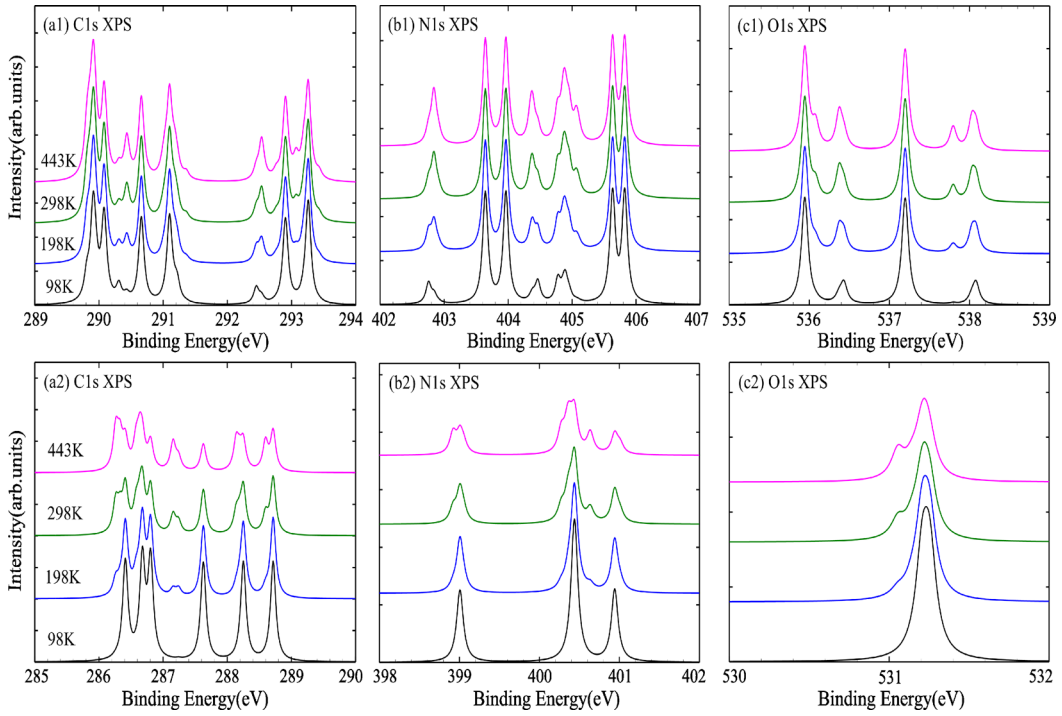

Figure 5. Calculated averaged XPS spectra at the (a) C, (b) N, and (c) O K-edges of neutral (top) and deprotonated (bottom) arginines at different temperatures.

4. CONCLUSION

To summarize, we have conducted a first-principles study on the K-edge NEXAFS spectra of neutral arginine in the solid phase as well as the XPS spectra of neutral, deprotonated, and protonated arginines in the gas phase. Solid-state calculations are based on one fixed crystal-structure geometry, while the gas-phase spectra are computed as an average over a few lowest-lying structures weighted by their equilibrium populations. Structure−property relation has been carefully examined by studying the influences of the intra-and intermolecular hydrogen bonds (HBs) as well as different charge states. In the NEXAFS spectra, our calculations show a visible difference for the canonical and zwitterionic forms of neutral arginine especially in the N edge. The solid-state effect does not lead to much visual changes in the π^* region, but individual transitions from different atoms can be strengthened or weakened (C edge); while the σ^* regions at all edges become much broader as expected. We also illustrate the functional dependence of X-ray absorption spectra in this ionic crystal, which is slightly more evident in the C edge. With the XPS study, we find that the canonical and zwitterionic forms show even more evident difference, which suggests a possible way to clearly distinguish the dominant form in the gas phase. We also find that deprotonation and protonation always lead to red and blue shifts of several electronvolts of the core binding energies at all edges. The normal hydrogen bond Y−H···X (X, Y = N, O) has a different influence on the binding energies of the hydrogen acceptor X and donor Y and, respectively, cause a blue and red shift of about 1 eV. The weak C−H···Y hydrogen bond also leads to a weak red shift (less than 1 eV) of the C1s binding energies. By comparing the averaged spectra of both the neutral and the deprotonated arginines at four different temperatures, we find that a lower temperature does not introduce many changes in peak positions, while the peaks become much sharper and some small structure features disappear. Our results provide a better understanding of the influences of the intra- and intermolecular forces on the electronic structure of arginine.

AUTHOR INFORMATION

Corresponding Author

*E-mail: luo@theochem.kth.se.

Notes

The authors declare no competing financial interest.

ACKNOWLEDGMENTS

This work is supported by the State Key Development Program for Basic Research of China (2010CB923300 & 2012CB215405), National Natural Science Foundation of China (20925311 & 11074233), and Göran Gustafsson Foundation for Research in Natural Sciences and Medicine. The Swedish National Infrastructure for Computing (SNIC) is acknowledged for computer time.

REFERENCES

(1) Stöhr, J. *NEXAFS Spectroscopy*; Spring Verlag: Berlin, Heidelberg, NY, 1992.
(2) Slaughter, A. R.; Banna, M. S. *J. Phys. Chem.* **1988**, *92*, 2165.
(3) Chong, D. P. *Can. J. Chem.* **1996**, *74*, 1005.
(4) Plashkevych, O.; Carravetta, V.; Vahtras, O.; Ågren, H. *Chem. Phys.* **1998**, *232*, 49.
(5) Gordon, M. L.; Cooper, G.; Morin, C.; Araki, T.; Turci, C. C.; Kaznatcheev, K.; Hitchcock, A. P. *J. Phys. Chem. A* **2003**, *107*, 6144.
(6) Jiemchooroj, A.; Ekström, U.; Norman, P. J. *Chem. Phys.* **2007**, *127*, 165104.
(7) Plekan, O.; Feyer, V.; Richter, R.; Coreno, M.; de Simone, M.; Prince, K. C.; Carravetta, V. *J. Phys. Chem. A* **2007**, *111*, 10998.
(8) Plekan, O.; Feyer, V.; Richter, R.; Coreno, M.; de Simone, M.; Prince, K. C.; Carravetta, V. *J. Electron Spectrosc. Relat. Phenom.* **2007**, *155*, 47.

(9) Plekan, O.; Feyer, V.; Richter, R.; Coreno, M.; de Simone, M.; Prince, K. C.; Carravetta, V. *Chem. Phys. Lett.* **2007**, *442*, 429.
(10) Feyer, V.; Plekan, O.; Richter, R.; Coreno, M.; Prince, K. C.; Carravetta, V. *J. Phys. Chem. A* **2008**, *112*, 7806.
(11) Feyer, V.; Plekan, O.; Richter, R.; Coreno, M.; Prince, K. C.; Carravetta, V. *J. Phys. Chem. A* **2009**, *113*, 10726.
(12) Zhang, W.; Carravetta, V.; Plekan, O.; Feyer, V.; Richter, R.; Coreno, M.; Prince, K. C. *J. Chem. Phys.* **2009**, *131*, 035103.
(13) Messer, B. M.; Cappa, C. D.; Smith, J. D.; Drisdell, W. S.; Schwartz, C. P.; Cohen, R. C.; Saykally, R. J. *J. Phys. Chem. B* **2005**, *109*, 21640.
(14) Messer, B. M.; Cappa, C. D.; Smith, J. D.; Wilson, K. R.; Gilles, M. K.; Cohen, R. C.; Saykally, R. J. *J. Phys. Chem. B* **2005**, *109*, 5375.
(15) Aziz, E. E.; Ottosson, N.; Eisebitt, S.; Eberhardt, W.; Jagoda-Cwiklik, B.; Vacha, R.; Jungwirth, P.; Winter, B. *J. Phys. Chem. B* **2008**, *112*, 12567.
(16) Grasjo, J.; Andersson, E.; Forsberg, J.; Duda, L.; Henke, E.; Pokapanich, W.; Bjorneholm, O.; Andersson, J.; Pietzsch, A.; Hennies, F.; Rubensson, J. E. *J. Phys. Chem. B* **2009**, *113*, 16002.
(17) Ottosson, N.; Børve, K. J.; Spångberg, D.; Bergersen, H.; Sæthre, L. J.; Faubel, M.; Pokapanich, W.; Öhrwall, G.; Björneholm, O.; Winter, B. *J. Am. Chem. Soc.* **2011**, *133*, 3120.
(18) Carravetta, V.; Plashkevych, O.; Ågren, H. *J. Chem. Phys.* **1998**, *109*, 1456.
(19) Mochizuki, Y.; Ågren, H.; Pettersson, L. G. M.; Carravetta, V. *Chem. Phys. Lett.* **1999**, *309*, 241.
(20) Zubavichus, Y.; Zharnikov, M.; Schaporenko, A.; Grunze, M. *J. Electron Spectrosc. Relat. Phenom.* **2004**, *134*, 25.
(21) Otero, E.; Urquhart, S. G. *J. Phys. Chem. A* **2006**, *110*, 12121.
(22) Boese, J.; Osanna, A.; Jacobsen, C.; Kirz, J. *J. Electron Spectrosc. Relat. Phenom.* **1997**, *85*, 9.
(23) Kaznacheyev, K.; Osanna, A.; Jacobsen, C.; Plashkevych, O.; Vahtras, O.; Ågren, H.; Carravetta, V.; Hitchcock, A. P. *J. Phys. Chem. A* **2002**, *106*, 3153.
(24) Zubavichus, Y.; Schaporenko, A.; Grunze, M.; Zharnikov, M. *J. Phys. Chem. A* **2005**, *109*, 6998. The experimental NEXAFS spectra of arginine in Figures 1−3 therein have been recaptured in our Figure 1
(25) Chapo, C. J.; Paul, J. B.; Provencal, R. A.; Roth, K.; Saykally, R. J. *J. Am. Chem. Soc.* **1998**, *120*, 12956.
(26) Rak, J.; Skurski, P.; Simons, J.; Gutowski, M. *J. Am. Chem. Soc.* **2001**, *123*, 11695.
(27) Ling, S.; Yu, W.; Huang, Z.; Lin, Z.; Haranczyk, M.; Gutowski, M. *J. Phys. Chem. A* **2006**, *110*, 12282.
(28) Goldberg, D. E. In *Genetic Algorithm in Search, Optimization and Machine Learning*; Addison-Wesley Publishing Company, Inc.: Reading, MA, 1989.
(29) Schlund, S.; Muller, R.; Grabmann, C.; Engels, B. *J. Comput. Chem.* **2008**, *29*, 407.
(30) Joseph, J.; Jemmis, E, D. *J. Am. Chem. Soc.* **2007**, *129*, 4620.
(31) Yu, W.; Lin, Z.; Huang, Z. *Chem. Phys. Chem.* **2006**, *7*, 828.
(32) Nordling, C.; Hagström, S.; Siegbahn, K. *Z. Physik.* **1964**, *178*, 433.
(33) Myneni, S.; Luo, Y.; Näslund, L. Å.; Cavallleri, M.; Ojamäe, L.; Ogasawara, H.; Pelmenschikov, A.; Wernet, Ph.; Väterlein, P.; Heske, C.; Hunssain, Z.; Pertersson, L. G. M.; Nisson, A. *J. Phys.: Condens. Matter* **2002**, *14*, L213.
(34) Wernet, Ph.; Nordlund, D.; Bergmann, U.; Cavalleri, M.; Odelius, M.; Ogasawara, H.; Näslund, L. Å.; Hirsch, T. K.; Ojamäe, L.; Glatzel, P.; Pertersson, L. G. M.; Nisson, A. *Science* **2004**, *14*, 995.
(35) Giuseppe, B.; Nadia, R.; Vincenzo, B. *Phys. Rev. Lett.* **2008**, *100*, 107401.
(36) Leetmaa, M.; Ljungberg, M. P.; Lyubartsev, A.; Nilsson, A.; Pettersson, L. G. M. *J. Electron Spectrosc. Relat. Phenom.* **2010**, *177*, 135.
(37) Hua, W.; Ai, Y.-J.; Gao, B.; Li, H.; Ågren, H.; Luo, Y. *Phys. Chem. Chem. Phys.* **2012**, *14*, 9666.
(38) Hetenyi, B.; Angelis, F. D.; Giannozzi, P.; Car, R. *J. Chem. Phys.* **2004**, *120*, 8632.
(39) Cavalleri, M.; Odelius, M.; Nordlund, D.; Nilsson, A.; Pettersson, L. G. M. *Phys. Chem. Chem. Phys.* **2005**, *7*, 2854.
(40) Prendergast, D.; Galli, G. *Phys. Rev. Lett.* **2006**, *96*, 215502.
(41) Chen, W.; Wu, X.; Car, R. *Phys. Rev. Lett.* **2010**, *105*, 017802.
(42) Kingsford-Adaboh, R.; Grosche, M.; Dittrich, B.; Luger, P. *Acta Crystallogr.* **2000**, *C56*, 1274.
(43) Hua, W.; Gao, B.; Li, S.; Ågren, H.; Luo, Y. *J. Phys. Chem. B* **2010**, *114*, 13214.
(44) Jolly, W. L.; Hendrickson, D. N. *J. Am. Chem. Soc.* **1970**, *92*, 1863.
(45) Davis, D. W.; Shirley, D. A. *Chem. Phys. Lett.* **1972**, *15*, 185.
(46) Best, P. E. *J. Chem. Phys.* **1972**, *49*, 2797.
(47) Plashkevych, O.; Privalov, T.; Ågren, H.; Carravetta, V.; Ruud, K. *Chem. Phys.* **2000**, *260*, 11.
(48) Brena, B.; Luo, Y.; Nyberg, M.; Carniato, S.; Nilson, K.; Alfredsson, Y.; Åhlund, J.; Mårtensson, N.; Siegbahn, H.; Puglia, C. *Phys. Rev. B* **2004**, *70*, 195214.
(49) Hua, W.; Yamane, H.; Gao, B.; Jiang, J.; Li, S.; Kato, H.; Kawai, T.; Luo, Y.; Kosugi, N.; Ågren, H. *J. Phys. Chem. B* **2010**, *114*, 7016.
(50) Nyberg, M.; Luo, Y.; Triguero, L.; Pettersson, L. G. M.; Ågren, H. *Phys. Rev. B* **1999**, *60*, 7956.
(51) Gao, B.; Wu, Z. Y.; Ågren, H.; Luo, Y. *J. Chem. Phys.* **2009**, *131*, 034704.
(52) Hua, W.; Gao, B.; Li, S.; Ågren, H.; Luo, Y. *Phys. Rev. B* **2010**, *82*, 155433.
(53) Frisch, M. J.; Trucks, G. W.; Schlegel, H. B.; Scuseria, G. E.; Robb, M. A.; Cheeseman, J. R.; Scalmani, G.; Barone, V.; Mennucci, B.; Petersson, G. A., et al. *GAUSSIAN 09*, revision A.02; Gaussian Inc.: Wallingford CT, 2009.
(54) Gao, B.; Jiang, J.; Liu, K.; Luo, Y. *BIONANO-LEGO*, version 2.0; Royal Institute of Technology: Sweden, 2008.
(55) Most individual $Z + 1$ calculations converge to restricted SCF solutions, while spin-polarized minima are achieved for terminal carbon (C_1 and C_6) excitations. The α and β electrons produce similar spectral shapes except a slight energy shift, and we simply use the averaged spectra. Wave functions are confirmed by stability tests.
(56) Lee, C.; Yang, W.; Parr., R. G. *Phys. Rev. B* **1988**, *37*, 785.
(57) Zhao, Y.; Truhlar, D. G. *Theor. Chem. Acc.* **2008**, *120*, 215.
(58) Kutzelnigg, W.; Fleischer, U. Schindler, M. *NMR-Basic Principles and Progress*; Springer-Verlag: Heidelberg, 1990; Vol. *23*, p 165.
(59) Uejio, J. S.; Schwartz, C. P.; Saykally, R. J.; Prendergast, D. *Chem. Phys. Lett.* **2008**, *467*, 195.
(60) Schwartz, C. P.; Uejio, J. S.; Duffin, A. M.; England, A. H.; Prendergast, D.; Saykally, R. J. *J. Chem. Phys.* **2009**, *131*, 114509.
(61) Uejio, J. S.; Schwartz, C. P.; Duffin, A. M.; England, A.; Prendergast, D.; Saykally, R. J. *J. Phys. Chem. B* **2010**, *114*, 4702.
(62) Schwartz, C. P.; Saykally, R. J.; Prendergast, D. *J. Chem. Phys.* **2010**, *133*, 044507.
(63) In fact, isomers Can3 and Z1 have relatively lower percent share values (3.3% and less than 1%, respectively, at 443 K). The inclusion of these isomers in this work is simply their peculiar structures. Note that Can3 has a different structure in the guanidine group compared with the other canonical isomers.
(64) Hermann, K.; Pettersson, L. G. M.; Casida, M. E.; Daul, C.; Goursot, A.; Koester,A.; Proynov, E.; St-Amant, A.; Salahub, D. R. *StoBe-deMon*, version 3.0; StoBe-deMon Software: Stockholm-Berlin, 2007.
(65) Becke, A. D. *Phys. Rev. A* **1988**, *38*, 3098.
(66) Perdew, J. P. *Phys. Rev. B* **1986**, *33*, 8822.
(67) Triguero, L.; Plashkevych, O.; Pettersson, L. G. M.; Ågren, H. *J. Electron Spectrosc. Relat. Phenom.* **1999**, *104*, 195.
(68) Bagus, P. *Phys. Rev.* **1965**, *139*, A619.
(69) Triguero, L.; Petersson, L.G. M.; Ågren, H. *Phys. Rev. B* **1998**, *58*, 8097.
(70) Takahashi, O; Pettersson, L. G. M. *J. Chem. Phys.* **2004**, *121*, 10339.
(71) Hua, W. *Structure and spectroscopy of bio- and nano-materials from first-principles simulations*, Ph.D. dissertation, Royal Institute of Technology, Stockholm, 2010; pp 38.

(72) Hagstrom, S.; Nording, C.; Siegbahn, K. *Phys. Lett.* **1964**, *9*, 235.